Tomislav Medić*, Christoph Holst, Jannik Janßen, and Heiner Kuhlmann

Empirical stochastic model of detected target centroids: Influence on registration and calibration of terrestrial laser scanners

https://doi.org/10.1515/jag-2018-0032
Received August 2, 2018; accepted March 6, 2019

Abstract: The target-based point cloud registration and calibration of terrestrial laser scanners (TLSs) are mathematically modeled and solved by the least-squares adjustment. However, usual stochastic models are simplified to a large amount: They generally employ a single point measurement uncertainty based on the manufacturers' specifications. This definition does not hold true for the target-based calibration and registration due to the fact that the target centroid is derived from multiple measurements and its uncertainty depends on the detection procedure as well. In this study, we empirically investigate the precision of the target centroid detection and define an empirical stochastic model in the form of look-up tables. Furthermore, we compare the usual stochastic model with the empirical stochastic model on several point cloud registration and TLS calibration experiments. There, we prove that the values of usual stochastic models are underestimated and incorrect, which can lead to multiple adverse effects such as biased results of the estimation procedures, a false a posteriori variance component analysis, false statistical testing, and false network design conclusions. In the end, we prove that some of the adverse effects can be mitigated by employing the a priori knowledge about the target centroid uncertainty behavior.

Keywords: terrestrial laser scanner, calibration, registration, stochastic model, target centroid detection

1 Introduction

Today, TLSs with their ability to rapidly acquire dense and high-quality 3D data are utilized as a standard tool for accurate geometry analysis in many applications [1]. TLSs are capable of detecting millimeter range deformations [2, 3] or even sub-millimeter rigid body movement of signalized targets, as it was demonstrated in [4, 5]. The detected target centroids of such signalized targets (Fig. 1) are often used for the tasks of the point cloud registration [6–8]. Moreover, because detecting the target centroid can reach even a submillimeter uncertainty [9], signalized targets are frequently used for TLS calibration [10–13], testing the geometric accuracy of TLSs [14], as well as to calibrate the mounting parameters between the TLS and the digital camera [15].

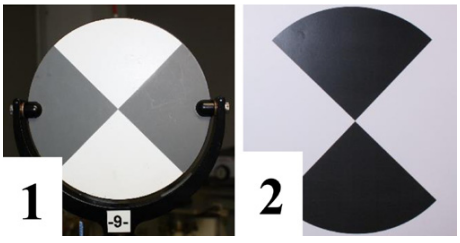

Figure 1: Commercially available targets used for calculating the uncertainty of the detected target centroid (1 – Leica Tilt and Turn target, 2 – self-printed A4 paper target with official Leica Black & White HDS template).

Both the target-based registration and the calibration rely on a well-established adjustment of point networks that are usually solved as the least-squares estimation problems, e. g. [16]. While there is no reason to question the validity of the functional model of the adjustment, the definition of a correct stochastic model should be discussed since, up to now, its impact on the results of calibration and registration has not been considered sufficiently in the literature.

The established approach of defining the stochastic model for such adjustments is founded on the process of converting Cartesian coordinates of the detected target centroid back to polar coordinates. Although estimated from multiple observations, target centroids are used to mimic the original instrument measurements [17]. Subsequently, the polar coordinates are associated with the measurement uncertainty described in the manufacturer's

***Corresponding author: Tomislav Medić,** Institute of Geodesy and Geoinformation, University of Bonn, Nussallee 17, 53115 Bonn, Germany, e-mail: t.medic@igg.uni-bonn.de
Christoph Holst, Jannik Janßen, Heiner Kuhlmann, Institute of Geodesy and Geoinformation, University of Bonn, Nussallee 17, 53115 Bonn, Germany, e-mails: c.holst@igg.uni-bonn.de, j.janssen@igg.uni-bonn.de, heiner.kuhlmann@igg.uni-bonn.de

specifications, which are optionally corrected using the variance component estimation (VCE). In the majority of the reviewed literature, this ends up to using constant scalar values defined for all ranges, horizontal and vertical angle measurements [18–22]. Although the stochastic model based on manufacturers' specifications comes close to reality and is sufficient for some applications, it does not quantify the true errors precisely:

- Specifications are often not perfectly transparent or they do not define the required information at all. For example, different manufacturers tend to use different descriptions of distance measurement uncertainty, which makes the derivation of the valid stochastic model challenging.
- The quality of the reflectorless electronic distance measurements (EDM) depends on many influencing factors, such as the measured distance, the angle of incidence and surface properties [23]. In addition, the quality of the detected target centroid depends on the selected measurement procedure (e. g. instrument settings). Hence, the association of a single scalar value for the uncertainty of all measurements introduces an error.
- Values in the specifications usually describe the single point uncertainty, while in the TLS registration and calibration, we rely on the target centroid, which is derived from multiple measurements. Hence, its uncertainty is expected to be lower than one from a single measurement.

In this work, we empirically derive a stochastic model that describes the precision of the detected target centroid. The model is valid for a certain combination of TLS, TLS settings, target centroid detection algorithm, and target pattern. The target centroid precision is described with respect to the measurement geometry (distance and angle of incidence) and it is compared with the usually employed stochastic models based on manufacturer's specifications (from now on noted as manufacturer's specification model or MSM). The empirical stochastic model (ESM) defined herein cannot be simply transferred to other combinations of instruments, targets, and algorithms. Hence, the intention of this paper is not to define a new stochastic model which is applicable to all TLS calibration and registration tasks. Rather, the main aims of the paper are:

- To indicate the differences between the uncertainty of the detected target centroid in reality and the uncertainty described in usual stochastic models. This includes the description of the uncertainty behavior of the target centroid with respect to the measurement configuration.
- To indicate all aspects, from network design to analysis of the results, which are influenced by inaccurate stochastic models and to quantify the influence of these models on the results of the TLS calibration and registration (using real datasets).
- To prove that a simple experimental setup for deriving the ESM in the form of the look-up tables can successfully mitigate some of the indicated adverse effects.

The paper is organized as follows. Section 2 explains the theoretical background of the study. In Section 3, the main mathematical relations are given. Section 4 describes the derivation of the empirical stochastic model and underlines the key differences in comparison to the previously established models. Section 5 presents calibration and registration related case studies based on the real data to reveal the possible influence of using an incorrect stochastic model. Finally, in Section 6, the main conclusions are drawn.

2 Theoretical background

Due to the fact that the uncertainty of the target centroid depends, among others, on the detection process, Section 2.1 gives a short overview of the target centroid detection algorithms and a more detailed explanation of the algorithm used within this study. Additionally, herein we reason the decision to empirically derive the stochastic model for the TLS target-based calibration and registration. Further, Section 2.2 explains the main concept of the ESM and theoretically reasons the presumptions necessary for the derivation of the ESM. Finally, in order to set a foundation for a discussion of the case studies (Section 5), Section 2.3 gives an exhaustive overview of all aspects of the TLS calibration and registration influenced by inaccurate stochastic models.

2.1 Target centroid detection algorithm

The TLS samples the surrounding with the regular grid of horizontal and vertical angular steps and records the measured distance and the intensity values describing the power of the received laser beam. Usually, the measured intensity values undergo unknown processing steps before they are available to the end user. Afterward, the original polar measurements (distances, horizontal and vertical angles) are transformed in Cartesian coordinates. Again, measurements interpolation and eventual correction steps are unknown to the end user. The end product

is the point cloud defined by the Cartesian coordinates and colored according to the processed intensity values.

In order to accurately detect the target centroid, the point cloud of a single target needs to be extracted from the whole point cloud (Fig. 2.a). Several algorithms were proposed so far for the automatic recognition and extraction of the point clouds associated with a single target [24–26]. However, within this study, that step is conducted manually. The following step is the accurate target centroid detection. Most of the commercially available targets used for terrestrial laser scanning are realized as planar contrast targets with differently colored regions (e. g. Figure 1). Different colors have an impact on the recorded intensity value (Figure 2) and this property is used to aid the target centroid detection. There are different algorithms proposed for the latter task. Most of the algorithms are based on edge detection followed by circle fitting [27] or searching for line intersections, e. g. [5, 25, 28–30]. An alternative to these approaches are the algorithms based on the template matching [24, 31]. The algorithm used in this study is based on the template matching algorithm described in [31] with some minor modifications.

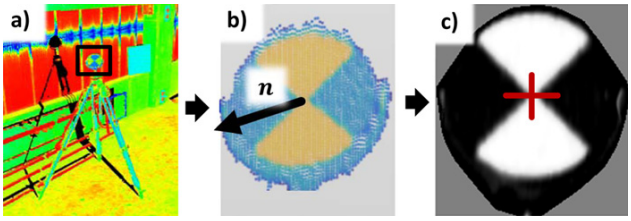

Figure 2: Simplified scheme of the target centroid detection: a) target extraction from the point cloud, b) best-fit-plane estimation (***n*** – plane normal vector), c) target centroid detection in the rasterized image (red cross – target centroid).

First, all points not belonging to the planar target are detected and removed using an initial best-fit-plane algorithm based on RANSAC method. The estimation of the target plane parameters is refined using the best-fit-plane algorithm based on the Gauss-Helmert-Model. Here, Cartesian coordinates are recalculated to polar coordinates and the observations are weighted based on the values described in the manufacturer's specifications. The intensity values of the original point cloud are projected onto the estimated plane in the direction of the measured distances, forming a rasterized intensity image (Fig. 2.c). Afterward, a template image of a target pattern is formed and the correlation coefficients between the template and the intensity image are calculated for each possible position of the template in the intensity image. The accurate position of the target centroid is determined by the greatest value of the correlation coefficient. Finally, the 2D coordinates of the target centroid are recalculated back to the 3D Cartesian coordinates. We would like to point out that the more detailed description of the in-house build target centroid detection algorithm, together with the detailed analysis of the achievable accuracy will be the part of the following publication.

The uncertainty of the target centroid is affected by the aforementioned processing steps. The exact approaches for the plane estimation, image rasterization, and centroid detection vary between different algorithms and for the commercial software they are unknown to the end user. Additionally, the quality of the intensity image used to detect the centroid depends on the instrument properties (measurement uncertainty, angular steps, divergence angle), selected settings (resolution, measurement filtering, beam power) and measurement configuration. Finally, the success of the target centroid detection also depends on the properties of the used target (size, pattern, color, material).

Hence, the uncertainty of the detected target centroid depends on multiple factors and it can hardly be derived analytically. Quantifying the share of each individual factor in the overall uncertainty budget has small practical relevance to the results of the TLS calibration and registration. Therefore, a detailed investigation of each uncertainty factor is beyond the scope of this research. Instead, we focus on revealing the difference between the empirically estimated uncertainty of the target centroids and the uncertainty values which are usually used in stochastic models for the TLS calibration and registration. Additionally, we propose an empirically derived stochastic model to accurately describe the overall uncertainty of the target centroid, without an in-depth analysis of the underlying factors. The proposed stochastic model will be discussed further in the following sections.

2.2 Target centroid detection accuracy and precision

The empirical stochastic model derived in this study describes the precision of the detected target centroid with respect to the measurement geometry. In order to justify this choice, we need to answer the following two questions:

- Is it acceptable to use the target centroid precision for deriving the stochastic model of TLS calibration and registration?
- Why should the target centroid precision be described with respect to the measurement geometry?

Regarding the first question, the main difference between calculating the target centroid precision and accuracy is that for the accuracy we need to consider both random and systematic errors, while for the precision considering only random errors is sufficient. We can divide all systematic effects influencing TLS measurements into four groups: instrumental misalignments, external influences, measurement geometry and effects related to measured object properties [23].

Firstly, the instrument misalignment errors are included in the functional model of the calibration, and, thus, they are eliminated. In the case of the scanner registration, they are mitigated using two-face measurements by a large amount.

Secondly, the external influences (atmospheric influence, refraction, earth's curvature) have a very small influence on the typical scanning distances for the panoramic laser scanners (1–100 m) and, thus, can be neglected [32].

Thirdly, object properties are constant for all targets for one calibration or registration task, if the targets of the same type are used. Hence, systematic effects act similarly on all of the measurements and they do not bias the results or they are absorbed in the estimated calibration parameters. Namely, the rangefinder offset in the TLS calibration is always said to be estimated for the scanner-target combination [16].

Lastly, systematic influences related to the measurement geometry can be decomposed on the effects due to differing distances and due to different incidence angles [33]. An eventual systematic effect of differing distances can be described by the scale parameter and it can be included in the functional model (not detected for the scanner under investigation). Thus, the only remaining systematic effect that can impact the accuracy of the target centroid is the effect of the incidence angle. It has been observed in [34] as a significant systematic influence and could be tackled by including an additional error term in the functional model. However, a proper functional model for this effect is still missing. Therefore, this step was not conducted in this study. Hence, it is the only factor expected to make a difference between the target centroid accuracy and the observed precision.

Therefore, based on this explanation, we expect our presumption that the target centroid precision is sufficient for deriving the empirical stochastic model to be justified. In any case, it is reasonable to expect that our stochastic model comes closer to explaining the true target centroid stochastic behavior than merely drawing values from manufacturer's specifications.

Regarding the second question, the measurement configuration or geometry is defined by two values: the scanner to target distance and the angle of incidence [33]. An impact of the increasing distance and the angle of incidence on the uncertainty of the detected target centroid in the range direction can be expected due to the worse signal to noise ratio [35] and it was already considered in some TLS calibration cases [13]. However, this effect is reduced in comparison to a single point measurement due to the abundant number of measurements used to estimate the target plane. This is especially true for close distances. The further the target is placed with respect to the scanner, the more prominent is the effect.

One of the possible ways of describing the precision of the target centroid in the range direction would be using an intensity based stochastic model for EDM measurements as introduced in [35]. However, this stochastic model describes the precision of the single range measurement, while the target plane is usually estimated from hundreds of measurements. The straightforward solutions could be just to divide the value from the intensity based stochastic model by the square root of points used for estimating the plane parameters or to use the a posteriori variance of the best-fit-plane parameters. However, both solutions result in overestimating the precision due to the neglected correlations between adjacent measurements [36]. Hence, we expect that using precision values based on empirical data presents a more realistic solution for the stochastic model of the target centroid.

In the case of angular measurements of the target centroid, the decrease of the precision due to the increase of incidence angle and the distance is never considered in the literature. Namely, most of the current literature bypasses the fact that the target centroid is not equivalent to the single point measurement. Angular measurements of a single point are influenced only by the noise of angular encoder readings and the remaining influence of mechanical misalignments. However, the target centroid is estimated using the intensity information recorded by the EDM unit for multiple points. This estimation heavily relies on the accurate differentiating between black and white parts of the target. This ability to differentiate between fields of different intensity is reduced with higher distances and incidence angles. This happens due to a less number of points in the point cloud and due to the higher footprint area of the reflected laser beam. Hence, in the case of the target centroid angular precision, the influence of measurement geometry should also be reflected.

These facts should be considered both for planning and for the analysis of TLS measurements and this will be discussed in the following section.

2.3 Adverse effects of an incorrect stochastic model

Knowledge about the true measurement uncertainty is necessary for several reasons. First, it is a crucial piece of information for the design and optimization of geodetic networks [37]. In the concrete case of TLSs, this information is required for deciding the best scanner and target locations for the TLS registration and calibration. The goal of the network optimization is to minimize the uncertainty of the estimated calibration parameters, in the case of TLS calibration, or transformation parameters, in the case of TLS registration. This optimization procedure can be described as searching for the optimal configuration matrix $\boldsymbol{A}$, while other input parameters are retained fixed [37]. In the literature, it is called the first order design (FOD) and it is a well-established geodetic task, unavoidable in the cases when the high product quality is demanded. Analogously, the knowledge of the true measurement uncertainty is also required for the third order design (TOD), which deals with the optimal densification of the existing networks.

Second, correct stochastic information is necessary for searching the optimal covariance matrix of measurements or the second order design (SOD) – [37]. In this case, optimal refers to the optimal ratio between cost efficiency (measurement time and necessary equipment) and the required measurement uncertainty. Hence, knowledge about the measurement uncertainty is required for the selection of an adequate scanner, scanner settings, targets and software for achieving the required product quality.

Third, using the correct stochastic model is a necessary prerequisite for the successful utilization of least-squares or robust adjustment algorithms. An incorrect a priori stochastic information can lead to several adverse effects. The most prominent one is biased parameter estimates in case of an incorrect distribution of the relative measurement weights within the network of observations [36]. Furthermore, incorrect prior information about the measurement uncertainty causes unrealistic values in the covariance matrix of the estimated parameters and leads to an incorrect a posteriori variance analysis and statistical testing results. Finally, if robust estimation algorithms are used, the outlier detection threshold is always bound to the expected measurement uncertainty (Section 3.2). Hence, if the a priori uncertainty is under or overestimated, wrong measurements are removed or retained.

To conclude, a good understanding of the anticipated measurement uncertainty is required for effective planning, processing, and analysis of geodetic measurements. In the case of the target-based TLS calibration and registration, this presumes knowledge about the quality of the detected target centroid. In the following sections, we will demonstrate how knowledge of the true measurement uncertainty impacts the planning of TLS measurements (FOD, SOD, TOD) and quantify the impact of different stochastic models on the processing and analysis of TLS calibration and registration.

3 Mathematical relations

For the complete understanding of the case studies (Section 5) used to test the hypothesis of this work, Sections 3.1 and 3.2 describe the adopted TLS target-based calibration and registration algorithms, which are based on least-squares and robust estimation methods. Additionally, in order to improve the statistical power of the estimated ESM, we grouped the results of multiple observations (Section 4). Hence, Section 3.3 explains the statistical concept used for the latter process.

3.1 Registration and calibration algorithms

The target-based TLS registration algorithm is generally based on the functional model of a rigid body transformation [38]. The goal of the approach is a simultaneous registration of local coordinate systems associated with each scanner station into a reference system of choice. The solution is usually obtained in a sense of least-squares minimization with a sufficient number of corresponding targets in each local coordinate system. The estimated parameters usually include both transformation parameters as well as target coordinates in the reference system

$$\boldsymbol{f}_j^i = \boldsymbol{R}^i_{(k,\phi,\omega)}\boldsymbol{xyz}_j^i + \boldsymbol{T}^i_{(X,Y,Z)} - \boldsymbol{XYZ}_j^{ref.} = \boldsymbol{0}, \tag{1}$$

where $i = 1, 2 \ldots, s$; $j = 1, 2 \ldots, p$; s and p are total numbers of scanner stations and targets used in the experiment. The estimated parameters are separated in the rotation matrix $\boldsymbol{R}^i_{(k,\phi,\omega)}$ defined with Euler angles (k, ϕ, ω), the translation vector $\boldsymbol{T}^i_{(X,Y,Z)}$ and the vector of Cartesian coordinates of targets in the reference system $\boldsymbol{XYZ}_j^{ref.}$. The measurement vector from the scanner station i to the target j in the local coordinate system is equal to

$$\boldsymbol{xyz}_j^i = \begin{bmatrix} x_j^i \\ y_j^i \\ z_j^i \end{bmatrix} = \begin{bmatrix} (r_j^i + \Delta r_j^i)sin(\theta_j^i + \Delta\theta_j^i)sin(\varphi_j^i + \Delta\varphi_j^i) \\ (r_j^i + \Delta r_j^i)sin(\theta_j^i + \Delta\theta_j^i)cos(\varphi_j^i + \Delta\varphi_j^i) \\ (r_j^i + \Delta r_j^i)cos(\theta_j^i + \Delta\theta_j^i) \end{bmatrix}, \tag{2}$$

where x_j^i, y_j^i, z_j^i are Cartesian coordinates of the target which are transformed to the polar coordinates r_j^i, φ_j^i, θ_j^i describing the genuine range, horizontal and vertical angle measurements, while Δr_j^i, $\Delta\varphi_j^i$, $\Delta\theta_j^i$ are measurement or registration errors. The polar coordinates are recalculated from the Cartesian coordinates using the following relations:

$$r_j^i = \sqrt{x_j^{i2} + y_j^{i2} + z_j^{i2}}, \tag{3}$$

$$\varphi_j^i = arctan\left(\frac{x_j^i}{y_j^i}\right), \tag{4}$$

$$\theta_j^i = arccos\left(\frac{z_j^i}{r_j^i}\right). \tag{5}$$

We use a least-squares adjustment realized as rigorous Gauss-Helmert model, introduced in TLS related applications in [39], which can be written in a matrix form as:

$$\boldsymbol{B}\boldsymbol{v} + \boldsymbol{A}\Delta\boldsymbol{x} + \boldsymbol{w} = \boldsymbol{0}. \tag{6}$$

Here $\boldsymbol{B}$ and $\boldsymbol{A}$ are Jacobian matrices with respect to the observations and the estimated parameters, $\boldsymbol{v}$ is the vector of residuals, $\boldsymbol{\Delta x}$ is the vector of reduced parameters, and $\boldsymbol{w}$ is the misclosure vector.

The single difference between registration and calibration algorithm is that the registration errors Δr_j^i, $\Delta\varphi_j^i$, $\Delta\theta_j^i$ (Eq. 2) are treated as solely random values (measurement residuals $v_{r_j^i}$, $v_{\varphi_j^i}$ and $v_{\theta_j^i}$) in the registration algorithm, but they are decomposed in a systematic and a random part in the calibration algorithm (Eq. 7–9). In the latter case, the number of unknown parameters is expanded for the calibration parameters describing the mentioned systematic part of the registration errors. In this study, we adopt the set of calibration parameters describing the mechanical misalignments of panoramic laser scanners which originates from [40] and it is adapted for the scanner used in this experiment (Leica ScanStation P20) as written in [21]:

$$\Delta r_j^i = x_2 sin\left(\theta_j^i\right) + x_{10} + v_{r_j^i}, \tag{7}$$

$$\Delta\varphi_j^i = \frac{x_{1z}}{r_j^i tan(\theta_j^i)} + \frac{x_3}{r_j^i sin(\theta_j^i)} + \frac{x_{5z-7}}{tan(\theta_j^i)} + \frac{2x_6}{sin(\theta_j^i)} + \frac{x_{1n}}{r_j^i} + v_{\varphi_j^i}, \tag{8}$$

$$\Delta\theta_j^i = \frac{x_{1n+2}cos(\theta_j^i)}{r_j^i} + x_4 + x_{5n}cos\left(\theta_j^i\right) - \frac{x_{1z}sin\left(\theta_j^i\right)}{r_j^i} - x_{5z}sin\left(\theta_j^i\right) + v_{\theta_j^i}. \tag{9}$$

Table 1: Calibration parameters describing relevant misalignments of Leica ScanStation P20.

Parameter	Description
x_{1n}	Horizontal beam offset
x_{1z}	Vertical beam offset
x_2	Horizontal axis offset
x_3	Mirror offset
x_4	Vertical index offset
x_{5n}	Horizontal beam tilt
x_{5z}	Vertical beam tilt
x_6	Mirror tilt
x_7	Horizontal axis error (tilt)
x_{10}	Rangefinder offset

The list of the parameters is presented in Table 1. Several parameters from the table are combined into one parameter because their separation induces either singularity or bias in the calibration adjustment [21].

For more information about each individual parameter, readers are referred to [40]. Herein, they will not be explained in detail, as they are not in the main focus of this study.

The local coordinate systems of each scanner station are defined as right-handed, Y – headed, clockwise rotating coordinate systems. This definition follows the true behavior of the instrument used in this experiment. The calculated horizontal angles are corrected for each quadrant by adding 180° or 360° where necessary, and the vertical angles are corrected by subtracting the calculated value from 360° where necessary. More information about the functional model of the adjustment process, the selected calibration parameters and the transformation of the Cartesian to polar coordinates can be found in [21]. Since the stochastic model used in these adjustments is the main focus of this study, it will be discussed in detail in sections 4 and 5.

3.2 Robust estimation

The measurements used in the previously explained adjustment (Sec. 3.1) can be influenced by gross errors. Hence, they might contain outliers, which change the distribution of the observations [41]. Taking this into account is important because least-squares estimates are known to be sensitive to outliers. Furthermore, the influence of outliers can be spread over many observations making them very difficult to detect [42]. In order to tackle this problem, a robust parameter estimator has been implemented in the algorithm when necessary (Sec. 5.2), as an estimator insensitive to outliers in observations.

In this study, we implemented the robust parameter estimator based on the Danish method [42], which was already introduced in TLS calibration in [39]. The advantages of this estimator are fast convergence, easy implementation in the least-squares adjustment and the fact that the estimates are equal to least-squares estimates if the observations are free from outliers. It is numerically realized as iteratively reweighted least-squares: first, the least-squares adjustment from Section 3.1 is realized using an a priori defined stochastic model (either ESM or MSM). Subsequently, the new weight matrix, which is called the equivalent weight matrix [43], is computed with the following weights based on the adjustment residuals:

$$p_i = \frac{1}{\sigma_i^2} exp\left(-\frac{v_i^2}{(3\sigma_i)^2}\right) \quad \text{if } |v_i| \geq 3\sigma_i, \tag{10}$$

$$p_i = \frac{1}{\sigma_i^2} \quad \text{if } |v_i| < 3\sigma_i. \tag{11}$$

Here, σ_i and v_i are the a priori defined standard deviation and the adjustment residual of the scanner measurement i. Hence, measurements having residuals exceeding a priori expected values are considered as outliers, their weights are reduced and their influence on the estimated parameters is also reduced. To avoid wrong outlier detection, the complete vector of residuals is tested in all iterations, leading to repeated reweighting of the complete covariance matrix. The reweighting starts after the second estimation of the unknown parameters in the least squares adjustment (2^{nd} iteration), in order to avoid wrong outlier detection due to bad parameter approximate values. Therefore, the algorithm is forced to make a minimum of three iterations to assure that the implemented outlier removal strategy takes an effect and it is repeated until a convergence criterion is met. We tested several different convergence criteria, without significant changes in the results. In the end, due to the run-time advantage, we adopted the criterion that the calibration parameters should not change for more than $0.01''$ or 1 µm in two consecutive iterations. For more details about the implemented robust estimator, readers are referred to [39].

3.3 Pooled standard deviation

In order to estimate representative standard deviations for each measurement type (ranges, horizontal angles, and vertical angles), we use data collected in the experiment described in Section 4. The data is divided into groups of samples. Firstly, the standard deviation for each sample group is obtained. In the following step, all corresponding group standard deviations are combined in one representative standard deviation, the weighted pooled standard deviation. The weighted pooled standard deviation is calculated as a square root of the mean variance, weighted by the number of redundant samples in each sample group [44]:

$$\sigma_{pooled} = \sqrt{\frac{\sum w_i \sigma_i^2}{\sum w_i}}. \tag{12}$$

Here, $i = 1, 2 \ldots, k$ and k is the number of groups, σ_i^2 is the group variance and w_i is the group weight proportional to the number of the samples. This way of combining standard deviations gives more representative value for the standard deviation of the whole population and it improves statistical power.

4 Defining the empirical stochastic model

This section begins with a description of the experiment realized to define the ESM (Sec. 4.1). It is followed by the presentation of the experiment results and discussion of the result's influence on the relevant aspects of the TLS calibration and registration (Sec. 4.2).

4.1 Experiment outline

The instrument used in this investigation is the Leica ScanStation P20. It is a highly accurate middle range panoramic laser scanner with the maximum range of 120 m and field of view of 360° × 270°. In the experiment, we used both the highest (0.8 mm at 10 m) and the second highest resolutions (1.6 mm at 10 m) in order to test the change of the target centroid detection precision with different scanner settings. In each case, quality level 1 was used, which denotes that no measurement averaging was employed [45].

The experimental setup was designed as follows. Fifteen targets (Fig. 3), of two target types provided by the manufacturer (Fig. 1), were scanned from multiple distances (approximately 2, 5, 10, 15, 20, 35, 50, 75, 100 meters) with differing angles of incidence (from approximately 0° to 60°).

This measurement setup describes the majority of scanner-target configurations that can be found on a real job scene. Incidence angles higher than 60° were omitted due to the fact that this unfavorable measurement setup is already avoided in the reference literature [27] and in practice. On each distance, eight measurements of each target

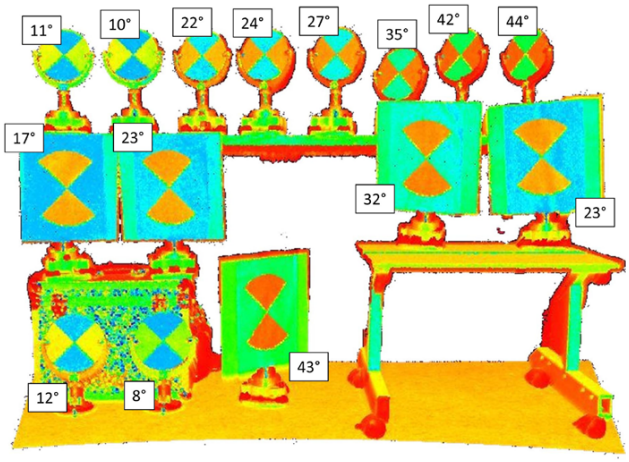

Figure 3: Point cloud of the experiment setup on the distance of 5 meters from the scanner (numbers denoting angle of incidence for each target in degree unit).

were repeated. The target centroids were detected using an in-house built algorithm (Section 2.1).

After the target centroid detection, coordinates of all centers were recalculated in polar coordinates (Eq. 3–5) in order to imitate original TLS polar measurements (r, φ, θ). We calculated the mean value of each polar measurement, we estimated the errors $(v_r, v_\varphi, v_\theta)$ for each measurement as a difference from the mean (Fig. 4). Then, we estimated the standard deviations of each polar measurement separately for each target. Hence, on each of the nine scanner-to-target distances, we estimated standard deviations for 15 targets. This resulted in 15 measurement groups (for each polar measurement) with corresponding standard deviations on each distance.

Initially, we pooled standard deviations of all 15 targets on each distance together in order to get the representative standard deviation for each distance (Eq. 12). The

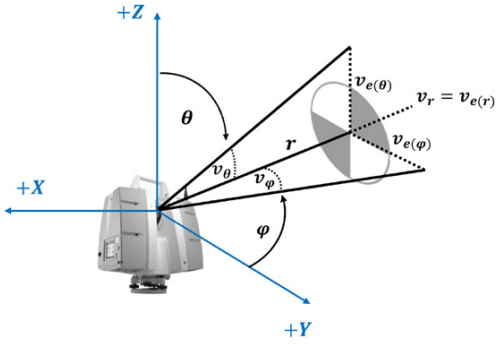

Figure 4: Errors of the estimated target centroid in range, horizontal angle and vertical angle direction $(v_r, v_\varphi, v_\theta)$ and corresponding Euclidian distance errors $(v_{e(r)}, v_{e(\varphi)}, v_{e(\theta)})$.

reason for such initial measurement grouping lies in the fact that we observed a high systematic relation between the standard deviation of the detected target centroid and the distance in all polar measurements. In addition, the understanding of the measurement uncertainty behavior with respect to the distance is mandatory information for the successful design of the optimal calibration or registration network. After deeper data analysis, we noticed the systematic relation between the measurement uncertainty and the incidence angle as well. Hence, in further processing, we pooled separately measurements of the targets with lower and measurements with higher incidence angles. This will be discussed in more detail in the following section.

4.2 Experiment results

The goal of this section is to present the results of the experiment described in the previous section, to underline the key differences between the proposed ESM and the usually employed MSM (Section 4.2.1) as well as to indicate how the results of this study relate to the different aspects of the TLS calibration and registration (Sections 4.2.2 and 4.2.3).

4.2.1 Comparison of ESM and MSM

If we decided to build up a stochastic model for the TLS target-based registration or calibration using the manufacturer's specifications, there are two different sources of information at hand for the given scanner (Leica ScanStation P20). First, there is a piece of information about the single point measurements, which gives values of $8''$ for the accuracy of angular measurements ($\sigma_\varphi = \sigma_\theta = 8''$) and 1 mm linearity error for EDM measurements ($\sigma_r = 1\,\text{mm}$) over the whole measurement range [46]. The information about the single point measurement quality is provided by the majority of the TLSs manufacturers and it is the most common way of building up a covariance matrix of observations in the literature [18–20]. In this case, two scalar values are used to describe the uncertainty of all detected target centroids within a certain job scene.

Second, for this particular scanner, there is stated a constant standard deviation of the detected target centroid of 2 mm up to distances of 50 m [46]. This value represents 3D Euclidian distance (spatial distance) in the local scanner coordinate system. In order to make the latter value comparable with the results of the experiment, we decomposed this spatial distance evenly into the direction of

three orthogonal axes. Namely, we decomposed it into the directions of range, horizontal and vertical angle measurements. Based on the law of variance propagation [47] the 1D uncertainty along each coordinate axis equals 1.16 mm. Hence, this results in the uncertainty of 1.16 mm in the latter three directions ($\sigma_{e(r)}, \sigma_{e(\varphi)}, \sigma_{e(\theta)} = 1.16\,\text{mm}$) indicated in Figure 4. As the input values of the calibration and registration algorithms are polar measurements, the related uncertainty in the covariance matrix of observation also needs to be recalculated into polar coordinates. Hence, the Euclidian errors $v_{e(\varphi)}$ and $v_{e(\theta)}$ are furtherly transformed in the angular errors (v_φ and v_θ), separately for each distance using the simple trigonometrical relations. For example, an error of 1.16 mm on 5 m distance corresponds to an angular error of $47.8''$, while the same error on 50 m distance corresponds to an angular error of $4.78''$.

Figure 5 represents the comparison of different uncertainty values that can be used to define the stochastic model for the target-based TLS calibration and registration:

- the single point measurement accuracy values provided in the manufacturer's specifications, which are usually used in the literature (MSM for the single point),
- the target centroid uncertainty provided in the manufacturer's specifications, which is available for the instrument under investigation, but it is not available for many instruments (MSM for the target centroid) and
- the empirically determined target centroid precision, as proposed within this study (ESM).

It is observable that using any of the latter information sources will lead to the notably different stochastic model. The ESM is represented with black curves, while MSM for the target centroid and MSM for the single point are represented with blue and red lines (or curves). The upper part of the figure shows the uncertainty of the distance measurements, while the middle and the lower part of the figure show the uncertainty of the horizontal angle measurements, first given in arc seconds and then in millimeters. The values for the vertical angle measurements are analog to the ones for the horizontal angle measurements, and hence, they are omitted.

As can be seen in Figure 5 (top), the uncertainty in the ranges is growing with the distance (ESM). In the case of the total station EDM measurements, the uncertainty is modeled with a constant value and a part linearly increasing with the distance, which is expressed as a ppm value [47]. However, it can be seen in the figure that even this linear representation is an oversimplification, as the observed uncertainty grows exponentially. In addition, on

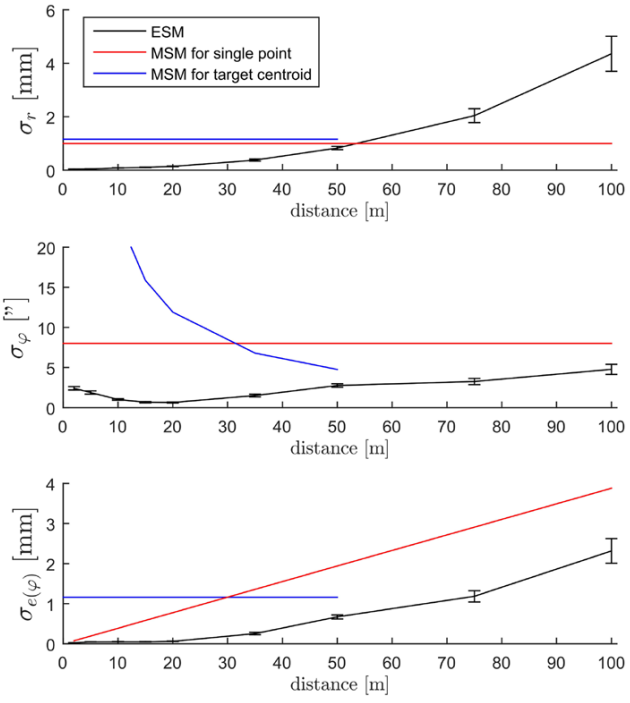

Figure 5: Comparison of the ESM with the stochastic models based on the data given in manufacturers specifications (using data for the single point and data for the target centroid). Error bars denoting values for one sigma.

the distances up to approximately 50 meters, the uncertainty is overestimated if we compare it with the uncertainty expected from both MSM. In contrary, the uncertainty is underestimated on the further distances. In the case of angular measurements, the uncertainty described by MSM is overestimated by a large amount on the whole measuring range (Fig. 5, middle).

These differences do not imply by any means that the values provided by the manufacturer are incorrect. They simply indicate that the values from the manufacturer's specifications do not accurately describe the uncertainty of the detected target centroid. This occurrence is not surprising. Namely, one of the values describes the accuracy of a single measurement, which does not correspond to the target centroid, while the other value is insufficiently precise. Hence, they are not perfectly suitable for deriving the stochastic model for TLS target-based calibration and registration approaches.

These differences directly lead to the overestimated registration and calibration parameter uncertainty based on the a posteriori variance component analysis. This can furtherly lead to incorrect statistical testing results. Additionally, it can lead to a wrong calculation of the point

cloud uncertainty if the uncertainties of the registration and calibration are furtherly propagated.

In addition, it should be pointed out that the angular uncertainty is not constant with the distance and it does not describe the straight horizontal line. In Figure 5, this deviation from linearity seems small, but it is significant and it represents the change in measurement uncertainty for more than 400 % in some cases. The dependency of the target centroid uncertainty on the measurement configuration will be furtherly discussed in Section 4.2.3.

These results prove that the stochastic model for the target centroid uncertainty is overly simplified by using the data provided in the manufacturer's specification. For highly demanding engineering tasks, such as the TLS calibration, this should not be neglected and the uncertainty of all measurements should not be represented with two or three scalar values. The expected measurement uncertainty should be drawn from look-up tables or represented with suitable functional models. The adverse effects of this oversimplification will be pointed out and quantified in the following sections.

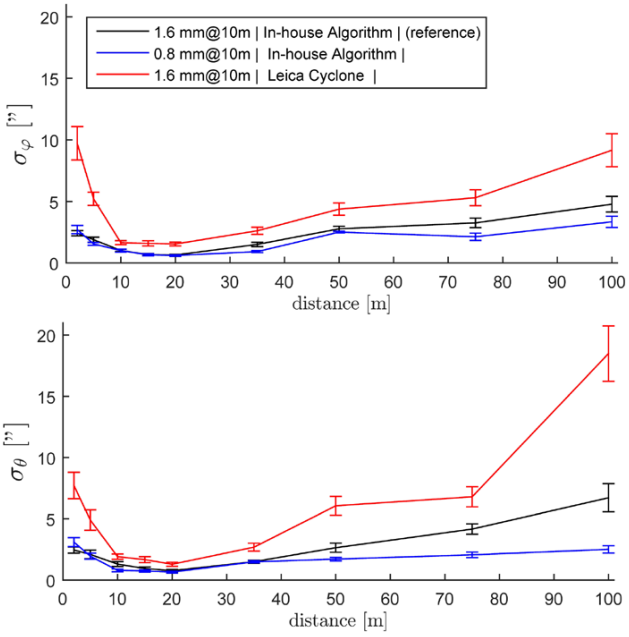

Figure 6: The change of the target centroid uncertainty behavior in the direction of horizontal and vertical angle measurements w. r. t. the scanning distance for different measurement procedures (altering resolution and algorithm). Error bars denoting values for one sigma.

4.2.2 Uncertainty and different measurement procedures – influence on SOD

As it was stated in the introduction, it is expected that the target centroid uncertainty depends on the different measurement procedures in the scope of different instruments, instrument settings, target design, and target centroid detection algorithm. In order to confirm these expectations, we estimated the target centroid uncertainty while altering different measurement procedures. The reference measurement procedure corresponds to the one described in Section 4.1. It includes using Leica ScanStation P20, the second highest resolution (1.6 mm at 10 m), the official Leica targets (Fig. 1) and the in-house built target centroid detection algorithm (Section 2.1). For the comparison, we individually altered the resolution settings (to the highest resolution of 0.8 mm at 10 m), and the algorithm (to Leica Cyclone).

The target centroid uncertainty in the direction of horizontal angles (top) and vertical angles (bottom) is presented in Figure 6. Each curve represents the uncertainty with different measurement procedure. Expectedly, the uncertainty notably changes if the procedure is altered. This holds true for all three measurement directions. This alternation is caused by changing the number of points used to sample the target (resolution) and the performance of the target centroid detection algorithm.

The presented results show the importance of understanding the accurate and robust uncertainty change with the different measurement processes. This knowledge aids cost-benefit analysis in the scope of optimizing equipment costs, measurement time and measurement quality. This task is one of the main responsibilities of geodetic engineers and it can be described as the second order design problem (SOD). Namely, altering the latter variables in the TLS measurement process directly induces different composition of the covariance matrix of observation in the TLS registration and calibration. For example, let us assume that we need to calibrate the scanner and the calibration parameters need to be estimated with a certain quality. Understanding the true uncertainty is necessary to make a decision which scanner settings, equipment, and software we need to use. For the particular example presented in Figure 6, it is visible that using a lower resolution does not lead to an increase of the target centroid uncertainty if the measurements are made on distances up to 35 m. For the scanner under investigation, that means that the measurement time in certain cases can safely be reduced by the factor of four, without any loss in the quality of the results. Hence, the oversimplification pointed out in the previous section leads to a sub-optimal solution of the second order design problem (in this case selection of measurement equipment and processing strategy).

4.2.3 Uncertainty and different measurement configuration – influence on FOD and TOD

Figure 7 represents the change of the uncertainty with respect to the measurement configuration for all three polar measurements (top to bottom: ranges, horizontal and vertical angles). In order to indicate the change of the uncertainty with respect to the incidence angle, we separated the scanned targets (Fig. 3) in two groups – one with lower incidence angles (0°–30°) and one with higher incidence angles (30°–60°). Consequently, we estimated two separated curves (blue and red) and we compare them with the curve estimated using all targets (black). A much larger number of measurements would be mandatory for the better modeling of the functional connection between the incidence angle and the measurement uncertainty. Such a measurement campaign was not possible at this point due to time constraint and, hence, it was omitted herein.

A clear systematic offset between the curves representing targets with different incidence angles is visible. The uncertainty of the targets with higher incidence angles (red) is always higher than the uncertainty of the targets with low incidence angles (blue). This indicates that when using the detected target centroids for registration or calibration, one should always consider an increase of the uncertainty with increasing incidence angle. And this holds true not only for the measurements in direction of ranges but horizontal and vertical angles as well.

As it was indicated previously, the uncertainty of the detected target centroid changes with respect to the distance (Sec. 4.2.1). In each case, this change is rather complex and it should be taken into account via look-up tables or appropriate functional models. Regarding the curve of angular uncertainty, there is a global curve minimum in which we can expect the lowest angular uncertainty. It can be clearly observed that the lowest angular uncertainty is achieved, in this instance, at approximately 20 m distance, both for horizontal and vertical angle measurements.

This phenomenon is explainable with the standard deviation of an arbitrary mean estimated from n samples. Figure 8 (top) depictures the standard deviation of the mean against a number of samples, where the standard deviation of each sample equals 1 (in arbitrary units). As it is known from the law of variance propagation [47], an improvement in the mean uncertainty with a higher number of samples is limited, and after a certain point, it reaches a plateau of nearly constant values.

The analog phenomenon can be observed for the standard deviation of the target centroid on short distances (2–20 m). The blue curve in Figure 8 (bottom) depictures the standard deviation of the target centroids in the di-

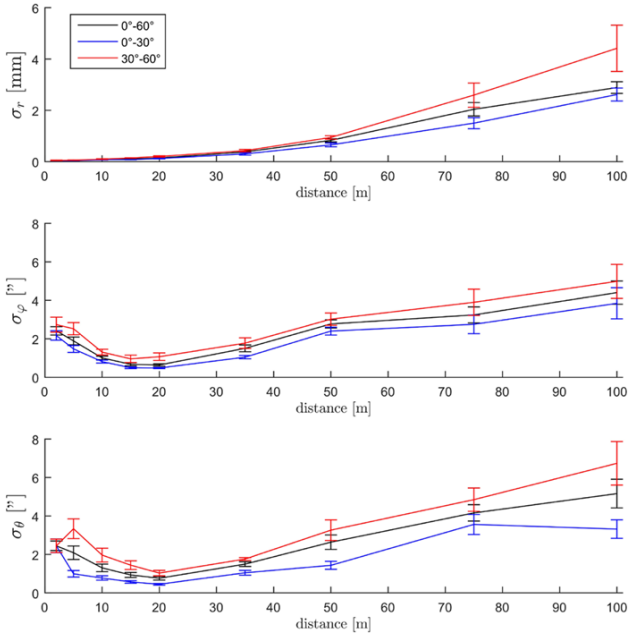

Figure 7: The change of the uncertainty behavior in the direction of ranges, horizontal and vertical angles w. r. t. the scanning distance: black – all targets used (incidence angles from 0° to 60°), blue – only targets with lower incidence angles used (0°–30°), red – only targets with higher incidence angle used (30°–60°). Error bars denoting values for one sigma.

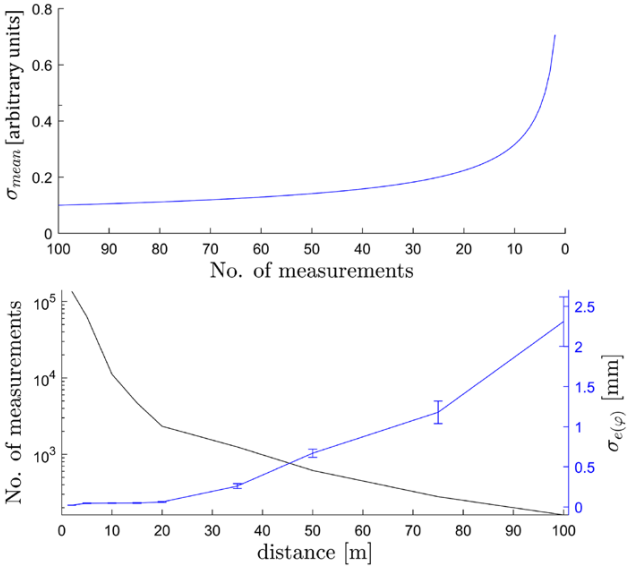

Figure 8: The change of the target centroid uncertainty with the distance. The upper part shows the increase in the uncertainty of the mean with the decrease of the measurements. The lower part shows the increase of the uncertainty of the target centroid (blue) with the decrease of the measurements (black). Error bars denoting values for one sigma.

rection of horizontal angles in millimeters (equivalent to the black curve in Figure 5, bottom). It is plotted against the number of measurements used to render the target intensity image (black curve). Again, when a certain number of measurements is reached, the uncertainty improvement reaches a plateau. When this nearly constant metric uncertainty (2–20 m) is recalculated into angular values, it causes an apparent decrease of the angular uncertainty with the distance (black curve in Fig. 5, middle). If the number of measurements drops under a certain value, a slope in the metric uncertainty gets steeper, and the angular uncertainty also starts to increase. Therefore, for a precise estimation of the target centroid, a number of measurements (therefore a resolution of the intensity image) has a higher importance than an accuracy of the individual TLS measurement. To conclude, the global minimum of the angular uncertainty is conditioned with the growth rate of the metric uncertainty. It would be interesting to observe how much the global minimum changes for different instruments. However, that is out of the scope of this work.

The latter phenomenon has a direct impact on the design and optimization of geodetic networks, more precisely on the first and third order design (FOD and TOD). Namely, in the process of planning the TLS measurement network for calibration field, two goals are pursued: realizing low measurement uncertainty and potentiating the effect of the scanner misalignments that are being modeled. The latter effect is proportionally growing with the distance for a large part of the calibration parameters.

Similarly, when planning a registration task, we tend to realize the lowest measurement uncertainty with the simultaneous realization of long distances (lever arms) between the targets. Namely, the estimated registration parameters are more accurate, if the targets are distributed over the larger surface. From Figure 7, it is visible that these criteria are best met somewhere around 20 m from the scanner under investigation for both tasks. Therefore, the knowledge of the true target centroid uncertainty is directly applicable to the design of the optimal calibration field or registration network.

To conclude, the correct stochastic model for the detected target centroid should consider the changes in the uncertainty with respect to the measurement geometry. So far, in order to improve the initial stochastic model based on the manufacturer's specifications, some authors used the results of the a posteriori variance component analysis, e. g. [21, 39]. This strategy undoubtedly improves the stochastic model. However, it again presumes that all distance and angular measurements can be represented with a single scalar value and that is not in accordance with the data presented herein. Hence, a better a priori understanding of the detected target centroid uncertainty is necessary both for the correct measurement planning (FOD, SOD, and TOD), as well as measurement processing and the analysis of the results. In the next sections, we will demonstrate and quantify the adverse impact of using MSM instead of ESM.

5 The influence of ESM and MSM on the TLS calibration and registration

In this section, three examples are used to demonstrate the impact of using the ESM instead of established MSM. Examples are based on datasets collected in three different empirical experiments. Two examples are used as showcases for the TLS calibration and one for registration. The data is processed using the algorithm described in Section 3.1 if it is not stated otherwise. The scanner used in all examples is the Leica ScanStation P20 described in Section 4.1. For defining the MSM we use constant values for the standard deviation of 1 mm for ranges and $8''$ for angular measurements, in order to stay consistent with proceeding studies, which use mostly the data for the single point measurement uncertainty (Section 1). For the ESM, we use the values presented in Figure 7 as a look-up table. Hence, the standard deviation of each measurement is estimated individually using linear interpolation based on the data obtained within the experiment described in Section 4.1.

5.1 Example 1 – simplified TLS calibration

Figure 8 presents the sketch of a simple measurement configuration used in the first example. This measurement configuration is extracted from the Leica Check & Adjust field calibration procedure [48]. Using the latter procedure, several calibration parameters were estimated. We presume that the manufacturers have the best in-depth knowledge about the instrument behavior and that they are able to provide accurate estimates of the calibration parameters. Hence, we presume that the values estimated this way can be considered as true values for the further discussion.

Four Leica Tilt and Turn targets (1–4) are measured from two scanner stations (S1 and S2) using measurements in two-faces (Fig. 9). All targets were approximately on the

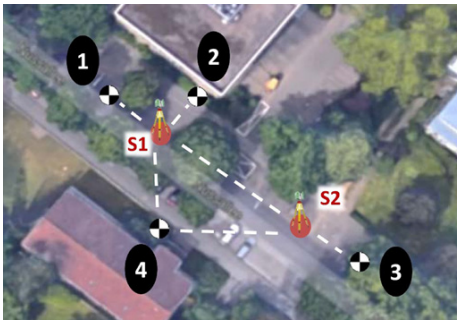

Figure 9: Sketch of the experiment used in 1st TLS calibration example. Four targets (1–4) measured from two scanner stations (S1 and S2).

horizon of the instrument for both scanner stations. Targets 1 and 2 are measured two times from Station S1. For the purpose of this demonstration, the measurements are separated into two groups – short distance measurements (approximately on 5 m) and long distance measurements (approximately on 20 m). When the measurements from both stations are combined, there are five two-face measurements on short (2*x* S1-1, 2*x* S1-2, S2-3) and five on long distances (S1-3, S1-4, S2-1, S2-2, S2-4). Finally, this whole measurement process is repeated four times with a time difference of one hour between each realization (datasets D1–D4).

The retrieved measurements are used for calculating two calibration parameters: vertical index offset and collimation axis error (x_4 and x_6 from Eq. 8–9). The parameters are estimated separately using the mean of the measurements on 5 m and the measurements on 20 m. They are calculated in accordance to the usual total station practice from the difference of two face measurements [47]. The results of this simplified calibration procedure for datasets D1–D4 are presented in Table 2.

Table 2: Vertical index offset (x_4) and collimation axis error (x_6) estimated using measurements on approximately 20 meters, 5 meters and reference results from Leica Check and Adjust field calibration procedure; results for four separate data sets (D1–D4), the corresponding mean and standard deviation.

Parameter	Data	D1	D2	D3	D4	$\bar{x}$	σ_x
x4 [″]	~ 20 m	−2.3	−2.4	−2.3	−1.9	−2.2	0.2
	~ 5 m	−0.5	−1.1	0.1	−0.2	−0.42	0.50
	Leica	−2	−2	−2	−1	−1.75	0.50
x6 [″]	~ 20 m	1.9	1.9	2.4	2.0	2.05	0.21
	~ 5 m	1.7	2.6	0.5	0.5	1.32	1.03
	Leica	2	2	2	1	1.75	0.50

As can be seen from Table 2, the standard deviations of the estimated parameters are higher if the measurements from the close distance are used. Hence, measurements in proximity to the scanner exhibit higher noise than measurements on the distance of approximately 20 meters. This behavior is in accordance with the ESM described in Section 4, and it is in accordance with the usual practice of a total station calibration. Namely, it is common knowledge in the geodetic community that for the better estimate of total station calibration parameters, the prism should be placed farther away from the instrument [47].

However, the stochastic models using a single scalar value for describing the uncertainty of angular measurements (e. g. MSM) do not reflect this phenomenon. This fact is very important for planning measurement networks and designing the calibration field. Namely, the majority of the documented TLS calibration experiments were conducted in relatively small rooms where a maximum achievable distance is approximately 10 meters, e. g. [16]. This further led to a suboptimal design of the TLS calibration fields with maximum lines of sights not exceeding more than three meters [22]. Based on the used functional models and available stochastic information, there were no indicators of the adverse effects of using such a small facility on the calibration results. In contrary, the results of this experiment suggest otherwise. For example, in the case of this concrete scanner, the vertical index offset is best estimated at a distance of approximately 20 meters, due to the smallest measurement uncertainty in the direction of vertical angles (Fig. 7). Additionally, if we compare the mean parameter values, it is visible that they fit closer to the true values if the measurements on high distances are used. Hence, using larger facilities for TLS calibration can significantly improve the calibration results and this fact should be considered in future TLS calibration projects.

To conclude, this simple calibration experiment indicates that the knowledge of the true measurement (target centroid) stochastic behavior is necessary for the successful planning and optimization of the TLS calibration networks.

5.2 Example 2 – TLS calibration

Figure 10 presents the network configuration used for the scanner calibration already described in [21]. Approximately 300 self-printed A4 paper targets with official Leica Black & White HDS template were regularly distributed in the large machine hall. The targets were measured from three scanner stations (S1, S2, and S3), where two-face measurements were used only from the first two stations.

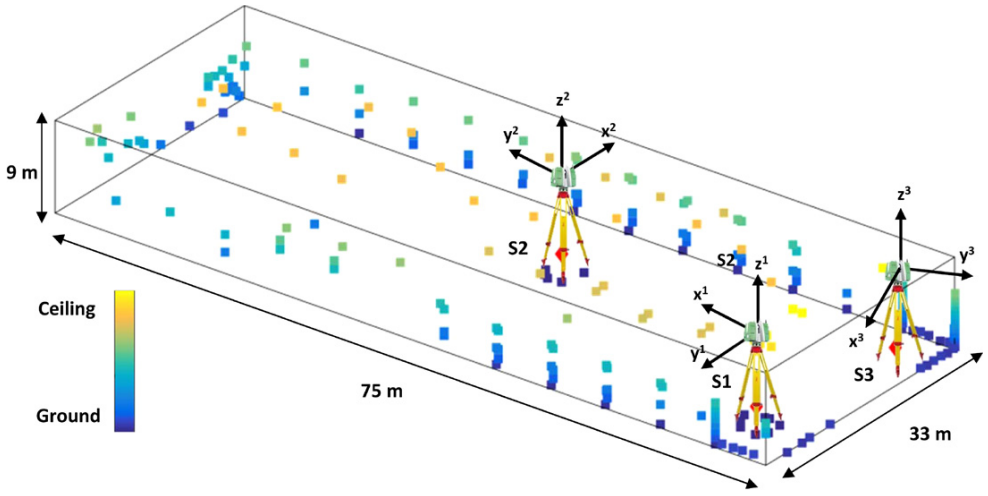

Figure 10: Network configuration – the scanner station locations (S1, S2, S3) with the orientation of scanner local coordinate systems and target distribution; hall dimensions 75 × 33 × 9 m.

[21] proved that the network is sensitive to all relevant calibration parameters (Eq. 7–9).

In order to ensure unbiased results, we eliminated all targets with incidence angles higher than 60° and all visually detectable outliers. To cope with the outliers that are not visually detectable, the calibration algorithm described in Section 3.1 was modified to a robust estimator using the Danish Method described in Section 3.2. This and similar robust estimation strategies are commonly employed for the scanner calibration in the literature ([12, 49]) due to the expected outliers that could bias the calibration results.

In order to compare the proposed empirical stochastic model with all of the usually employed stochastic models, the calibration adjustment was repeated three times. The first time, the ESM was used, the second time, the MSM was used, while the third time, the MSM was modified using the variance component estimation. The VCE is used iteratively to reweight the values in the covariance matrix of observations until the acceptance of the global test. The results of the adjustments are presented in Table 3 and Table 4. In Table 3, the a priori defined measurement standard deviations (forming the covariance matrix of observations) are compared with the a posteriori measurement standard deviations (based on the calibration adjustment residuals). The representative a priori standard deviation of the measurements for the ESM is calculated as the weighted pooled standard deviation of all measurements in the calibration field – separately for ranges, horizontal and vertical angles (Eq. 12). As it can be seen in Table 3, there is a much better correspondence between a priori and a posteriori values when the ESM or the MSM modified with the VCE are used. That means that both approaches can be used to describe the true behavior of the observation residuals more accurately. However, it should be noted that the MSM refined using the VCE does not account for the variability of the target centroid uncertainty with the different measurement geometry.

Table 3: Expected a priori standard deviations of TLS measurements vs. estimated a posteriori standard deviations of the calibration adjustment residuals. The results are presented for: the empirical stochastic model (ESM), the stochastic model based on the manufacturer's specifications (MSM) and the MSM modified using the variance component estimation.

		σ_r [mm]	σ_φ [″]	σ_θ [″]
ESM	a priori	0.29	1.68	1.53
	a posteriori	0.27	1.95	1.58
MSM	a priori	1.00	8.00	8.00
	a posteriori	0.27	3.26	1.75
MSM (VCE)	a priori	0.27	3.26	1.75
	a posteriori	0.24	2.66	1.25

A small discrepancy between the proposed ESM and the a posteriori values can be seen in the standard deviation of horizontal angle residuals. There is no directly applicable explanation for this and it should be further investigated. However, we expect that this behavior is connected to the systematic influence of incidence angles (Sec. 2.1). Namely, in the horizontal angle direction, there is high variability in the incidence angles, while there is very low variability in the vertical angle direction, which fits perfectly to our proposed stochastic model. The global test did not pass for the MSM and the ESM, despite the high

Table 4: Calibration parameters estimated using the ESM, the MSM, and the MSM modified with the VCE – MSM (VCE), the corresponding uncertainty and results of the significance testing with 99 % probability.

	Par.	x	σ_x	Sig.
	x10 [mm]	0.06	0.04	N
	x2 [mm]	−0.06	0.01	Y
	x1z [mm]	−0.05	0.02	Y
	x3 [mm]	−0.05	0.01	Y
	x5z7 [″]	−0.68	0.68	N
ESM	x6 [″]	1.82	0.05	Y
	x1n [mm]	−0.19	0.05	Y
	x4 [″]	7.19	0.07	Y
	x1n2 [mm]	0.17	0.01	Y
	x5n [″]	7.39	0.56	Y
	x5z [″]	−2.67	0.71	Y

					MSM (VCE)		
	Par.	x	σ_x	Sig.	x	σ_x	Sig.
	x10 [mm]	0.29	0.23	N	0.14	0.08	N
	x2 [mm]	0.06	0.05	N	0.04	0.01	Y
	x1z [mm]	0.14	0.07	Y	0.04	0.03	N
	x3 [mm]	0.00	0.03	N	−0.01	0.01	N
	x5z7 [″]	−8.51	3.13	Y	−4.23	1.32	Y
MSM	x6 [″]	1.59	0.24	Y	3.14	0.1	Y
	x1n [mm]	−0.10	0.25	N	−0.2	0.09	N
	x4 [″]	7.22	0.42	Y	7.25	0.09	Y
	x1n2 [mm]	0.14	0.05	Y	0.26	0.01	Y
	x5n [″]	8.49	3.08	Y	5.21	0.72	Y
	x5z [″]	−2.39	4.00	N	−1.96	0.90	N

correspondence between a priori and a posteriori values in the latter case.

Table 4 presents the estimated calibration parameters using all three stochastic models, estimated a posteriori standard deviations of the calibration parameters, and the result of the test of the parameter significance (one-tailed Student's t-test, 99 % significance). Utilizing this statistical test is not completely justified due to high correlations between the calibration parameters. However, we presented the results of the student t-test in order to demonstrate the influence of different stochastic models on the usual statistical parameter evaluation approaches [20].

As can be seen, some of the parameters have notably different values in all three cases. We tested if the whole sets of the calibration parameters are significantly different using the congruency test (test statistics compared with the value from the Fisher distribution) – [50]. The results of the test indicated that the parameters are significantly different with 99 % probability when different stochastic models are used (Tab. 5). Based on these results, it is not possible to determine which of the tested stochastic models leads to the estimation of unbiased calibration parameters. However, the results point out that the TLS calibration is very sensitive to the choice of the stochastic model. Additionally, it is demonstrated that using an inaccurate stochastic model can significantly bias the calibration results. Hence, great care should be placed in the derivation of the appropriate stochastic model for the TLS calibration.

Table 5: Congruency test used for evaluating if the calibration parameters estimated using the ESM are significantly different from the parameters estimated using the MSM (with and without the VCE) with 99 % probability (rejection signalizing significant difference).

	ESM vs. MSM	ESM vs. MSM (VCE)
Tc	2.30	9.32
$F(h, r, 1-\alpha)$	2.25	2.26

In addition, the a posteriori estimated parameter standard deviations are notably different when using different stochastic models. As expected, the highest differences are present when the simplistic MSM is compared with the proposed ESM or the MSM enhanced with the VCE. These differences can sometimes reach a factor of 6. Hence, using the MSM results in the overestimated uncertainty of the calibration parameters, while the other two stochastic models lead to the more realistic estimates. These different a posteriori parameter standard deviations again lead to different conclusions about the significance of individual parameters. In this instance, approximately half of the parameters have a different conclusion about their significance when the ESM is compared with other stochastic models. This can further lead to a wrong calculation of the single point uncertainty if the calibration parameter uncertainty is propagated to derive the point cloud uncertainty. Hence, these results point out how much the a posteriori variance component analysis and statistical testing are sensitive to the choice of the correct stochastic model.

Based on the results presented in Tables 3 and 4, it can be deduced that both the ESM and the MSM with the VCE offer more realistic estimates of the parameters' uncertainty and their significance. However, they are still different and, based on this experiment, it is impossible to deduce which of the two stochastic models is more accurate. What it is known is that the covariance matrix of the observations in the VCE case does not consider the relations between the target centroid uncertainty and the measurement geometry. Disregarding these relations can easily lead to biased estimates of the correlated calibration parameters. Namely, the calibration parameters typically share high mutual correlation and much research effort is

placed on their decorrelation [10, 18]. A further improvement in using the VCE could be achieved by introducing multiple measurement groups with a homogenous measurement geometry, and hence, with a corresponding target centroid uncertainty. Such a strategy would probably lead to values similar to the ones presented in Figure 7. Thus, this could be an alternative approach for deriving the ESM for the target centroid uncertainty. However, this requires a thorough investigation of the optimal number of measurement groups which could sufficiently represent the target centroid uncertainty behavior. Such a comprehensive investigation is out of the scope of this study.

To conclude, this example proves that using either the proposed ESM or the MSM improved with the VCE is necessary to get an accurate representation of the uncertainty of both the TLS observations and the estimated calibration parameters. Additionally, it revealed that using incorrect stochastic models can cause: significantly biased estimates of the calibration parameters, incorrect estimation of the parameters uncertainty and their significance. Therefore, sufficient attention should be placed on deriving an accurate stochastic model.

5.3 Example 3 – TLS registration

For the TLS registration example, we used a network adjustment consisting of 10 scanner stations (Fig. 11). An average distance between the stations is 100 meters and the whole length of the network is approximately 900 meters. The stations S1 and S10 are deliberately not connected through observing the same targets in order to enhance the transformation parameter errors. For the target-based registration of all scanner stations, Leica Tilt and Turn targets (Fig. 1) mounted on tripods were used, with minimally three corresponding targets between stations. The average of the two-face measurements is used to mitigate the influence of systematic TLS errors. The datum of the reference coordinate system of the measurement network is realized by treating coordinates of four targets at the beginning of the network as given values.

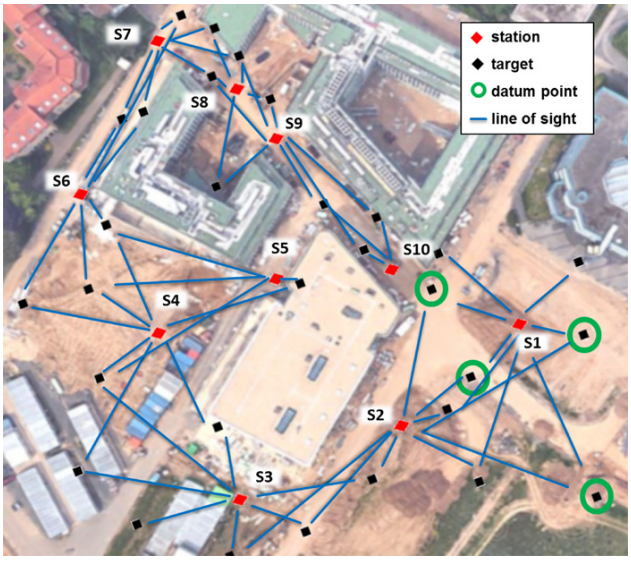

Figure 11: Measurement configuration of the network in the registration example (red rhombus – scanner stations, black squares – target locations, blue line – measurement directions, green circles – targets used for defining network datum).

The differences between the transformation parameters estimated using the ESM and the MSM are given in Table 6. As can be seen from the table, the parameter difference can rapidly build up reaching values of 18″ for the rotation and 13.4 mm for the translation parameters. Most of these values are higher than the calibration parameters estimated in the previous examples. Hence, they cannot be treated as insignificant in no case and they would have a notable influence on the results of the following point cloud analysis. The a posteriori parameter uncertainties were again different up to a factor of five for the ESM and the MSM. It is worth noting that this example presents a typical TLS project that can be expected in practice. Hence, the impact of the insufficient stochastic models can be visible even in the tasks not aiming at the highest reachable accuracy (e. g. TLS calibration).

As in the previous case study, we additionally tested the MSM modified by the VCE. This registration attempt delivered the same transformation parameters as the pro-

Table 6: Differences between transformation parameters estimated using ESM and MSM for all scanner stations (S1–S10).

	Δx^*				
Parameter	**S1**	**S2**	**S3**	**S4**	**S5**
T_x [mm]	0.12	−0.52	−3.44	**−4.46**	−0.93
T_y [mm]	−0.04	0.15	0.99	6.31	6.7
T_z [mm]	−0.01	0.03	−0.39	−0.65	−0.44
R_x [″]	−0.13	−0.09	−0.57	−1.48	−0.96
R_y [″]	−0.16	−1.37	−1.94	−1.27	−1.24
R_z [″]	−0.25	−8.76	**−18.68**	−17.53	−17.89
Parameter	**S6**	**S7**	**S8**	**S9**	**S10**
T_x [mm]	−5.04	−2.74	−1.18	−1.08	−0.53
T_y [mm]	10.26	**13.47**	12.44	11.82	9.91
T_z [mm]	−1.09	−1.19	0.11	1.02	**3.84**
R_x [″]	1.9	−7.19	0.32	4.99	**−8.06**
R_y [″]	−3.81	3.78	**−10.62**	−10.42	−9.11
R_z [″]	−14.69	−12.9	−11.98	−7.22	−9.6

$^*\Delta x = x(\text{MSM}) - x(\text{ESM})$

posed ESM (differences less than 0.02″ and 0.02 mm). Also, the transformation parameters uncertainties were at the same level of magnitude. This data shows that the estimation of the transformation parameters is less sensitive on the change of the target centroid uncertainty with different measurement geometry. Hence, if there is no necessity for the prior network design, the VCE can be utilized instead of the proposed ESM without any disadvantages.

Table 7: Expected a priori standard deviations of the TLS measurements according to the ESM, the MSM and the MSM modified with the VCE vs. estimated a posteriori standard deviation of the registration residuals.

		σ_r [mm]	σ_φ [″]	σ_θ [″]
ESM	a priori	0.41	1.82	1.59
	a posteriori	0.58	5.52	1.24
MSM	a priori	1.00	8.00	8.00
	a posteriori	0.41	5.12	1.13
MSM (VCE)	a priori	0.22	7.20	1.13
	a posteriori	0.22	7.20	1.13

In the end, the a priori and a posteriori measurement standard deviations are compared in Table 7. The a posteriori standard deviations in the range and vertical angle direction are consistent with the ESM. However, the horizontal angle uncertainty is much higher, probably due to excessive target rotations around standing axis between the consecutive scanner stations. Namely, the rotation of Tilt and Turn targets can introduce systematic errors with an unknown magnitude if the target center is not coincident with the center of the rotational axis (no values are given by manufacturer). This fact does not pose a problem in the previous examples, since calibration in the machine hall relies mostly on paper targets, while Tilt and Turn targets used in the previous experiment were not rotated during the measurements. Hence, the ESM does not describe the complete horizontal angle uncertainty in this concrete case. However, we use this example merely to show the possible impact of the different values in stochastic models on the transformation parameters estimated using the least-squares adjustment. Hence, this bias has no impact on the conclusions of the study. To conclude, a more rigorous target design is necessary for using the full potential of the precise TLS target centroid detection.

This example demonstrated that using the overly simplified stochastic model can influence the values of the registration parameters by a large amount. This influence can be characterized as a systematic error due to the incorrect registration and it can notably impact the point cloud uncertainty. Hence, it should not be neglected. As the TLS registration seems less sensitive on the choice of the stochastic model than the TLS calibration, both the proposed ESM and the MSM modified with the VCE lead to the same results.

6 Conclusion

We empirically investigated the precision of the target centroid detection and we defined an empirical stochastic model. Furthermore, we presented how using the inaccurate stochastic models can impact the TLS calibration and registration. Several important conclusions can be drawn from this study:

- The stochastic behavior of the detected target centroid is usually overly simplified and the uncertainty overestimated. Namely, the target centroid uncertainty depends on many influencing factors. It depends on the used measurement procedure (e. g. scanner settings and target centroid estimation algorithm) and it depends on the measurement configuration (distance and angle of incidence). This holds true for the uncertainty both in the direction of range and angular measurements. Hence, representation of the target centroid uncertainty in the stochastic models of the TLS calibration and registration by using constant scalar values is inadequate.
- Mentioned oversimplification has adverse effects on the tasks of planning, processing, and analysis of TLS measurements. We pointed out and quantified all adverse effects in the TLS calibration and registration workflows.
- Simple experimental setup and look-up tables with a linear interpolation can be used for obtaining more realistic stochastic information describing the target centroid uncertainty. The application of such stochastic information has a positive influence on the tasks of the first, second and third order design of the TLS calibration and registration.

The stochastic model derived herein can certainly be improved. For example, an influence of different incidence angles on the target centroid uncertainty can be investigated in more detail. Moreover, there is a possibility to functionally model the target centroid uncertainty instead of using look-up tables. The possibility to estimate an accurate stochastic model through variance component esti-

mation with multiple measurement groups should also be considered. However, this is beyond the scope of this work.

Regarding the relevance of the results, the use of signalized targets is still unavoidable in highly demanding engineering tasks due to a simple control with instruments of higher accuracy, and due to a straightforward estimation of the measurement uncertainty. Hence, the entire subject of the matter remains relevant in the geodetic community. Without correct stochastic models, there is no possibility of reaching millimeter or submillimeter uncertainties when analyzing the geometry of complex objects, which could be achievable in the near future. Therefore, we would recommend implementation of more complex stochastic models in the commercial software or the expansion of the values delivered in the instrument specifications in order to allow qualified professionals the possibility of more accurate data processing.

References

[1] W. Mukupa, G. W. Roberts, C. M. Hancock, and K. Al-Manasir, "A review of the use of terrestrial laser scanning application for change detection and deformation monitoring of structures," *Surv. Rev.*, vol. 49, no. 353, pp. 99–116, 2017.

[2] H. Yang, M. Omidalizarandi, X. Xu, and I. Neumann, "Terrestrial laser scanning technology for deformation monitoring and surface modeling of arch structures," *Compos. Struct.*, vol. 169, pp. 173–179, 2017.

[3] C. Holst, T. Medić, and H. Kuhlmann, "Dealing with systematic laser scanner errors due to misalignment at area-based deformation analyses," *J. Appl. Geod.*, vol. 12, no. 2, pp. 169–185, 2018.

[4] M. Tsakiri, D. Lichti, and N. Pfeifer, "Terrestrial laser scanning for deformation," *3rd IAG/12th FIG Symp.*, p. 10, 2006.

[5] J. C. K. Chow, W. F. Teskey, and J. W. Lovse, "In-situ Self-calibration of Terrestrial Laser Scanners and Deformation Analysis Using Both Signalized Targets and Intersection of Planes for Indoor Applications," in *14th FIG Symposium on Deformation Measurements and Analysis*, 2011.

[6] J. Pandžić, M. Pejić, B. Božić, and V. Erić, "Error model of direct georeferencing procedure of terrestrial laser scanning," *Autom. Constr.*, vol. 78, pp. 13–23, 2017.

[7] Z. Ji, M. Song, H. Guan, and Y. Yu, "Accurate and robust registration of high-speed railway viaduct point clouds using closing conditions and external geometric constraints," *ISPRS J. Photogramm. Remote Sens.*, vol. 106, pp. 55–67, 2015.

[8] B. Becerik-Gerber, F. Jazizadeh, G. Kavulya, and G. Calis, "Assessment of target types and layouts in 3D laser scanning for registration accuracy," *Autom. Constr.*, vol. 20, no. 5, pp. 649–658, 2011.

[9] L. Wang, B. Muralikrishnan, P. Rachakonda, and D. Sawyer, "Determining geometric error model parameters of a terrestrial laser scanner through two-face, length-consistency, and network methods," *Meas. Sci. Technol.*, vol. 28, no. 6, 2017.

[10] B. Muralikrishnan, L. Wang, P. Rachakonda, and D. Sawyer, "Terrestrial laser scanner geometric error model parameter correlations in the Two-face, Length-consistency, and Network methods of self-calibration," *Precis. Eng.*, vol. 52, pp. 15–29, 2017.

[11] M. A. Abbas, D. D. Lichti, A. K. Chong, H. Setan, and Z. Majid, "An on-site approach for the self-calibration of terrestrial laser scanner," *Meas. J. Int. Meas. Confed.*, vol. 52, no. 1, pp. 111-–123, 2014.

[12] Y. Reshetyuk, "A unified approach to self-calibration of terrestrial laser scanners," *ISPRS J. Photogramm. Remote Sens.*, vol. 65, no. 5, pp. 445–456, 2010.

[13] J. C. K. Chow, D. D. Lichti, C. Glennie, and P. Hartzell, "Improvements to and comparison of static terrestrial LiDAR self-calibration methods," *Sensors (Switzerland)*, vol. 13, no. 6, pp. 7224–7249, 2013.

[14] T. Kersten, K. Mechelke, M. Lindstaedt, and H. Sternberg, "Geometric accuracy investigations of the latest terrestrial laser scanning systems," *FIG Work. Week*, vol. June, pp. 1–16, 2008.

[15] M. Omidalizarandi and I. Neumann, "Comparison of Target- and Mutual Information Based Calibration of Terrestrial Laser Scanner and Digital Camera for Deformation Monitoring," *Int. Arch. Photogramm. Remote Sens. Spat. Inf. Sci.*, vol. 40, no. 1/W5, pp. 559–564, 2015.

[16] D. D. Lichti, "Error modelling, calibration and analysis of an AM-CW terrestrial laser scanner system," *ISPRS J. Photogramm. Remote Sens.*, vol. 61, no. 5, pp. 307–324, 2007.

[17] D. D. Lichti, "The impact of angle parameterisation on terrestrial laser scanner self-calibration," *Int. Arch. Photogramm. Remote Sens. Spat. Inf. Sci*, vol. 38, no. 3/W8, pp. 171–176, 2009.

[18] D. D. Lichti, "Terrestrial laser scanner self-calibration: Correlation sources and their mitigation," *ISPRS J. Photogramm. Remote Sens.*, vol. 65, no. 1, pp. 93–102, 2010.

[19] M. A. Abbas et al., "Improvements to the accuracy of prototype ship models measurement method using terrestrial laser scanner," *Meas. J. Int. Meas. Confed.*, vol. 100, pp. 301–310, 2017.

[20] J. L. Lerma and D. García-San-Miguel, "Self-calibration of terrestrial laser scanners: selection of the best geometric additional parameters," *ISPRS Ann. Photogramm. Remote Sens. Spat. Inf. Sci.*, vol. II-5, no. June, pp. 219–226, 2014.

[21] T. Medić, C. Holst, and H. Kuhlmann, "Towards System Calibration of Panoramic Laser Scanners from a Single Station," *Sensors*, vol. 17, no. 5, p. 1145, 2017.

[22] X. Ge, "Terrestrial Laser Scanning Technology from Calibration to Registration with Respect to Deformation Monitoring," Technical University of Munich, 2016.

[23] S. Soudarissanane, R. Lindenbergh, M. Menenti, and P. Teunissen, "Scanning geometry: Influencing factor on the quality of terrestrial laser scanning points," *ISPRS J. Photogramm. Remote Sens.*, vol. 66, no. 4, pp. 389–399, 2011.

[24] D. Akca, "Full Automatic Registration of Laser Scanner Point Clouds," *Opt. 3D Meas. Tech. IV*, vol. I, pp. 330–337, 2003.

[25] C. Yi et al., "Automatic Detection of Cross-Shaped Targets for Laser Scan Registration," *IEEE Access*, vol. 6, pp. 8483–8500, 2018.

[26] Y. Liang, Q. Zhan, E. Che, M. Chen, and D. Zhang, "Automatic Registration of Terrestrial Laser Scanning Data Using Precisely

Located Artificial Planar Targets," *IEEE Geosci. Remote Sens. Lett.*, vol. 11, no. 1, pp. 69–73, 2014.
[27] J. Chow, A. Ebeling, and T. Bill, "Low cost Artificial Planar Target Measurement Techniques for TLS," *FIG Congr. 2010 Facing Challenges – Build. Capacit.*, no. April 2010, p. 13, 2010.
[28] M. Omidalizarandi, J. Paffenholz, and I. Neumann, "Automatic and accurate passive target centroid detection for applications in engineering geodesy," *Surv. Rev.*, pp. 1–16, 2018.
[29] P. Rachakonda, B. Muralikrishnan, and D. Sawyer, "Metrological Evaluation of Contrast Target Center Algorithm for Terrestrial Laser Scanners," *Measurement*, no. 134, pp. 15–24, 2018.
[30] X. Ge and T. Wunderlich, "Target Identification in Terrestrial Laser Scanning," *Surv. Rev.*, vol. 47, pp. 129–140, 2014.
[31] K. Kregar, D. Grigillo, and D. Kogoj, "High precision target determination from a point cloud," *ISPRS Ann. Photogramm. Remote Sens. Spat. Inf. Sci.*, vol. II-5/W2, no. November, pp. 11–13, 2013.
[32] K. Kowalczyk and J. Rapinski, "Investigating the Error Sources in Reflectorless EDM," *J. Surv. Eng.*, vol. 140, no. 4, p. 6014002, 2014.
[33] S. Soudarissanane, "The geometry of terrestrial laser scanning; identification of errors, modeling and mitigation of scanning geometry," TU Delft, 2016.
[34] M. Zámecnikova, H. Neuner, S. Pegritz, and R. Sonnleitner, "Investigation on the influence of the incidence angle on the reflectorless distance measurement of a terrestrial laser scanner," *Vermessung Geoinf.*, no. 2+3, pp. 208–218, 2015.
[35] D. Wujanz, M. Burger, M. Mettenleiter, and F. Neitzel, "An intensity-based stochastic model for terrestrial laser scanners," *ISPRS J. Photogramm. Remote Sens.*, vol. 125, pp. 146–155, 2017.
[36] T. Jurek, H. Kuhlmann, and C. Holst, "Impact of spatial correlations on the surface estimation based on terrestrial laser scanning," *J. Appl. Geod.*, vol. 11, no. 3, pp. 143–155, 2017.
[37] E. W. Grafarend and F. Sanso, *Optimization and Design of Geodetic Networks*, 1st ed. Springer-Verlag Berlin Heidelberg, 1985.
[38] D. D. Lichti and J. Franke, "Self-Calibration of the iQsun 880 Laser Scanner," in *In Proceedings of the Optical 3-D 927 Measurement Techniques VII, Vienna, Austria*, 2005, pp. 122–131.
[39] Y. Reshetyuk, "Self-calibration and direct georeferencing in terrestrial laser scanning," KTH Stockholm, 2009.
[40] B. Muralikrishnan et al., "Volumetric performance evaluation of a laser scanner based on geometric error model," *Precis. Eng.*, vol. 40, pp. 139–150, 2015.
[41] K.-R. Koch, *Parameter Estimation and Hypothesis Testing in Linear Models*, 2nd ed. New York: Springer, 1999.
[42] T. Krarup, J. Juhl, and K. Kubik, "Götterdämmerung over least squares adjustment," in *14th Congress of ISPRS*, 1980.
[43] A. Wieser and F. K. Brunner, "Short Static GPS Sessions: Robust Estimation Results," *GPS Solut.*, vol. 5, no. 3, pp. 70–79, 2002.
[44] R. G. Lomax and D. L. Hans-Vaughn, *An Introduction to Statistical Concepts*, 3rd ed. New York: Taylor & Francis, 2012.
[45] E. Heinz, C. Holst, and H. Kuhlmann, "Erhöhung der räumlichen Auflösung oder Steigerung der Einzelpunktgenauigkeit beim Laserscanning – Analyse der Modellierungsgenauigkeit am Beispiel einer Ebene," in *Photogrammetrie Laserscanning Optische 3DMesstechnik – Beiträge der Oldenburger 3D-Tage*, 2018, pp. 167–179.
[46] Leica, "Leica ScanStation P20 Industry ' s Best Performing Ultra-High Speed Scanner," *Leica Scanstation P20 Datasheet*, 2015.
[47] W. Schofield and M. Breach, *Engineering Surveying*, 6th ed. Oxford: Elsevier, 2007.
[48] Leica, "Leica HDS Check & Adjust – User Manual," vol. 1, 2012.
[49] D. Garcia-San-Miguel and J. L. Lerma, "Geometric calibration of a terrestrial laser scanner with local additional parameters: An automatic strategy," *ISPRS J. Photogramm. Remote Sens.*, vol. 79, pp. 122–136, 2013.
[50] W. F. Caspary, *Concepts of network and deformation analysis*, 3rd ed. Sidney, Australia: School of Geomatic Engineering, University of New South Wales, 2000.